Mineralogical Magazine, 2014, Vol. 78(2), pp. 373–385

Local order in wüstite using a pair distribution function (PDF) approach

T. R. Welberry*, D. J. Goossens and A. P. Heerdegen

Research School of Chemistry, Australian National University, Canberra, ACT 0200 Australia

[*Received 13 October 2013; Accepted 19 November 2013; Associate Editor: S.J. Mills*]

ABSTRACT

We show how different aspects of a model of the complex disordered structure of wüstite, $Fe_{1-x}O$, affect the pair distribution function (PDF) and powder diffraction pattern. The aim is to assess the efficacy of using these techniques to determine details of local structure. The different aspects include the nature of the individual defect clusters, the nature of the paracrystalline superlattice on which they are distributed and the 'size-effect' relaxation of the basic rocksalt FeO matrix around the defects. The results show that PDF data are sensitive to those aspects of the models that have a significant effect on the populations of interatomic spacings but are less able to determine correlation structures in the samples if these do not have a substantial interaction with interatomic separations.

Keywords: local order, paracrystal, wüstite, pair distribution function.

Introduction

Many minerals (and materials more widely) show evidence of strong and complex local structural ordering. This local ordering can affect the mechanical properties of a material, the transport properties (for example, how vacancies relate to oxygen transport through the structure) and the thermodynamics, and so is clearly of prime importance. For crystalline materials the analysis of single crystal-diffuse scattering (SCDS) is the most definitive way of determining local structure but for many minerals (and materials more widely) single crystals of a sufficient size for such studies are often not readily obtainable and powder diffraction data must suffice. While conventional powder X-ray diffraction (XRD) (e.g. using Rietveld refinement – Rietveld, 1969) can provide information about the average crystal structure, total scattering (TS) – which includes both Bragg peaks and diffuse scattering – is needed if information about the local structure and short-range order is to be gained. The pair distribution function (PDF) analysis of such total scattering data has become a widely used technique for extracting such local structural information from a wide variety of materials including crystalline powders, nano-materials, amorphous materials, glasses and liquids (Michel *et al*., 2007; Juhas *et al*., 2006; Billinge and Levin, 2007; Proffen, 2006; Huq *et al*., 2010).

The aim of the present work is to explore the sensitivity of the PDF methodology to various aspects of disorder and short-range order for a mineral system for which the local structure has been characterized previously using SCDS. The system chosen for this study is the non-stoichiometric iron oxide wüstite, ($Fe_{1-x}O$, x = 0.057). The XRD patterns obtained from a single crystal of wüstite show strong and richly structured diffuse scattering (Fig. 1). This has enabled a detailed model of the defect structure to be established (Welberry and Christy, 1995,

* E-mail: welberry@rsc.anu.edu.au
DOI: 10.1180/minmag.2014.078.2.10

This paper is published as part of a special issue of *Mineralogical Magazine*, Volume **78(2)**, 2014, in celebration of the International Year of Crystallography.

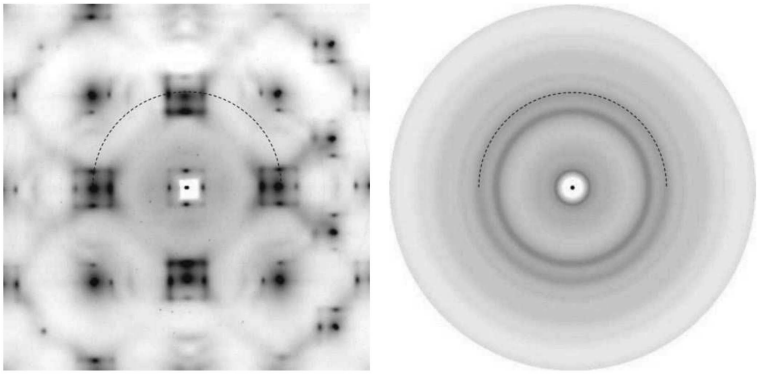

FIG. 1. (*a*) The richly structured diffuse scattering from a single crystal of wüstite, $Fe_{1-x}O$. (*b*) The same figure rotationally averaged to illustrate the apparent loss of detailed information that might be expected if only powder diffraction data are available.

1997). The aim is to assess to what extent this defect structure model could have been established using PDF analysis of powder diffraction data.

The approach adopted in this paper is as follows. The previously established model of wüstite is constructed progressively from its constituent parts and the PDF of the model calculated at each stage. In this way assessment is made as to which features of the defect model, all essential to reproduce the observed SCDS patterns, may be observed in the PDF and which features or attributes cannot.

The pair distribution function

The PDF makes use of the TS from a sample – all of the scattering that occurs continuously throughout reciprocal space. The TS is most often analysed within the PDF framework. The scattering is described by the function $S(Q)$,

$$S(Q) = \frac{I^{\mathrm{coh}}(Q) - \sum c_i |f_i(Q)|^2}{|c_i f_i(Q)|^2} + 1 \qquad (1)$$

where I^{coh} is the observed intensity at Q, the c_i are the atomic concentrations and the f_i are the X-ray form factors (neutron scattering lengths in the case of neutron diffraction). The pair distribution function, $G(r)$ is then calculated from

$$G(r) = \frac{2}{\pi} \int_{Q_{\min}}^{Q_{\max}} Q[S(Q) - 1] \sin(Qr) dQ \qquad (2)$$

where choice of $Q_{\min}$ and $Q_{\max}$ has an influence on the calculated $G(r)$ (Proffen and Billinge, 1999) and were chosen to be 0 and 26 $\mathrm{Å}^{-1}$ respectively, on the basis of typically used experimental values for X-ray total scattering.

For crystalline materials, the total scattering includes the sharp Bragg peaks that derive from the inherent periodicity but also includes the diffuse scattering that results from local departures from periodicity. For non-crystalline materials: amorphous materials, liquids, glasses and nanoparticles, all of the scattering is diffuse. The PDF makes use of finely powdered samples and hence the experiment yields a total scattering pattern that is a simple one-dimensional function. This means that the method is widely applicable and allows study of all the different kinds of materials listed above. However, for crystalline or even semi-crystalline materials it would seem that the spherical averaging could result in the loss of valuable information.

The disordered defect structure of wüstite

The structure of the non-stoichiometric oxide wüstite, $Fe_{1-x}O$, has been the subject of much debate over many years (Roth, 1960; Koch and Cohen, 1969; Garstein and Cohen, 1980; Schweika *et al*., 1995), largely because the details of the structure appear to depend heavily on the stoichiometry and thermal history of the sample (Welberry and Christy, 1998). However, a detailed model describing the defect structure for a particular single crystal sample of wüstite was developed some time ago (Welberry and Christy, 1995, 1997) and it is this model that will be considered in detail here. This model was able to

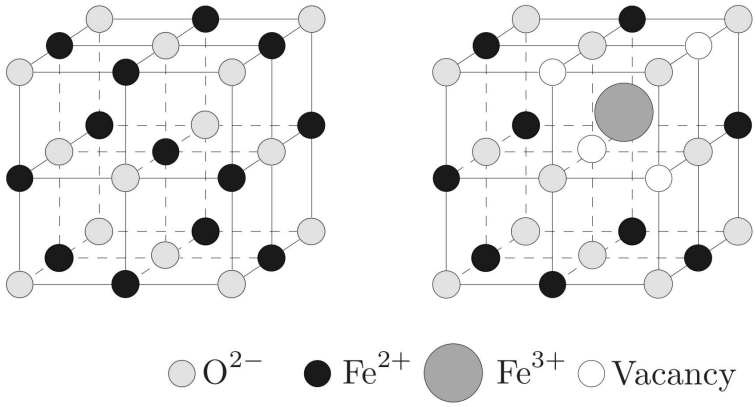

FIG. 2. The rocksalt structure (left) and a tetrahedral defect within it (right).

account convincingly for the observed single-crystal diffuse scattering data obtained from a crystal with stoichiometry $Fe_{1-x}O$, $x = 0.057$.

The model considers several different aspects of the disordered crystal, including the nature of the defect clusters, the distribution of the clusters over the crystal lattice and the manner in which the remainder of the crystal relaxes around these defects. Each of these different aspects can be parameterized, and different realizations of the model varying about the optimum solution can be obtained readily. By calculating both SCDS and PDF for a range of model realizations, we assess the sensitivity of PDF for characterizing the different aspects of the disordered model. We also explore the impact of the different aspects on $S(Q)$.

The average structure is of the rocksalt type with O^{2-} and Fe^{2+} ions each forming interpenetrating face-centred cubic (f.c.c.) sublattices. The O sublattice is treated as fully occupied, while the Fe sublattice contains vacancies (Hazen and Jeanloz, 1984). There are also Fe^{3+} ions on interstitial sites. It is likely that the Fe^{2+} vacancies and Fe^{3+} interstitials combine to form clusters. The smallest proposed cluster is the V_4T cluster consisting of 4 vacancies (V) forming a tetrahedron on neighbouring Fe^{2+} sites, together with one Fe^{3+} interstial (T) at the centre of the tetrahedron (Fig. 2). Modelling suggested that only the larger clusters, $V_{13}T_4$ and $V_{16}T_5$, were needed to model the data (Welberry and Christy, 1995, 1997). These larger clusters are made up of tetrahedral clusters in various corner-, edge- or face-sharing arrangements. Figure 3 shows these clusters. It should be noted that these three types of cluster are the smallest ones having cubic symmetry, but the presence of other lower symmetry clusters cannot be ruled out.

Figure 4*a* shows the X-ray SCDS pattern for the *hk*0 section of wüstite. This shows the reciprocal lattice of primary diffraction peaks corresponding to the f.c.c. rocksalt lattice. However, each of these spots is surrounded by a motif of scattering, containing subsidiary peaks, which derives from the distribution of defect clusters. In fact the clusters are arranged on an incommensurate 'superlattice'. This superlattice is a primitive lattice of average spacing $\sim 2.7\mathbf{a}_0 \times 2.7\mathbf{a}_0 \times 2.7\mathbf{a}_0$, where $\mathbf{a}_0$ is the basic rocksalt lattice parameter. However, Fig. 4*b* shows an enlargement of one motif and it is apparent that the superlattice peaks are broad, anisotropic and connected by diffuse streaking. This indicates that the superlattice is not perfectly regular but has considerable variation both in the length and direction of its basic lattice vectors. This kind of distorted lattice can be described by a paracrystal model (Welberry *et al*., 1980).

Three parameters are used to specify this paracrystal. σ^2 is the variance of the displacement of an individual lattice site away from the ideal regular lattice position and ρ_T and ρ_L are transverse and longitudinal correlation coefficients that describe the extent to which the displacements of neighbouring sites are coupled. The values of these three parameters in the previously developed model (Welberry and Christy, 1995, 1997) were $\sigma = 0.315$; $\rho_T = 0.935$; $\rho_L = 0.8$. In the section on different paracrystal distributions, we will also make use of ρ_D, which is the 'diagonal' correlation, in

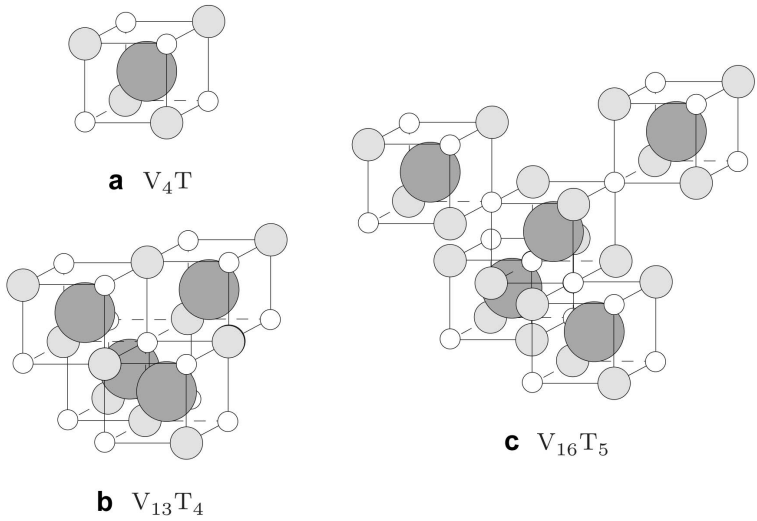

FIG. 3. Three possible defect clusters, with the larger ones being built up from edge- or corner-connecting V_4T clusters. Each cluster shows cubic symmetry. The differently shaded circles have the same meaning as in Fig. 2

between 'T' and 'L'. Where it is not used, it is allowed to arise as a consequence of ρ_T and ρ_L. Note that the value of σ gives the magnitude of the lattice-point displacements as a fraction of the lattice repeat-distance; $\sigma = 0.0$ would correspond to a perfect superlattice array of defects.

Another key result of the SCDS analysis (Welberry and Christy, 1997) was that, in order to explain the strong diffuse peak that occurs at the centre of the scattering motif, it is necessary for the crystal to be inhomogeneous, with some regions having the perfect rocksalt structure while others contain the paracrystalline array of defect clusters. To model this, the paracrystal array of defects is assumed to be either present or absent by referring to a second independent distribution on the same lattice. For this second distribution, a simple binary Ising model is used. The Ising spin variable $\sigma_{i,j}$ (= ±1) is used to designate whether defect clusters on the paracrystal lattice are

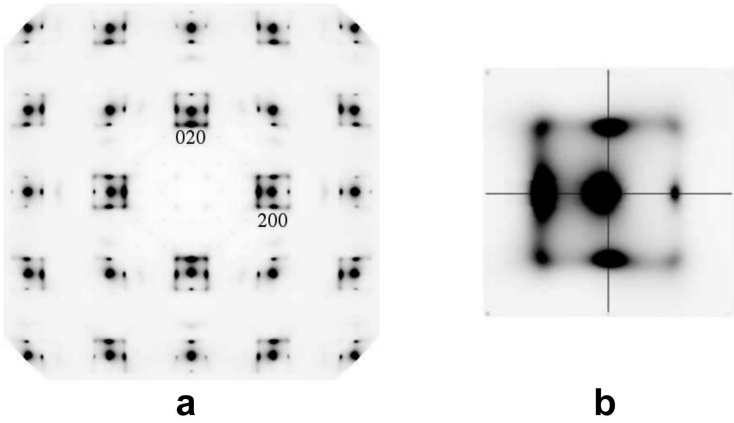

FIG. 4. Observed XRD patterns of wüstite. (*a*) The *hk*0 cut of reciprocal space, (*b*) a close-up view of the motif of scattering around the 200 Bragg reflection. Data were recorded at the 11-ID-B beamline at the Advanced Photon Source using 58.26 keV X-rays ($\lambda = 0.2128$ Å).

present ($\sigma_{i,j} = +1$) or absent ($\sigma_{i,j} = -1$). Ising model realizations can be generated with varying degrees of local order (or domain size) and these are then used in conjunction with the paracrystal lattice to obtain the final defect distributions. The degree of order or domain size can be specified by the nearest neighbour correlation ($C_{10} = <\sigma_{i,j}\sigma_{i-1,j}>$).

Finally, it is noted from Fig. 4 that the motifs of scattering around the different rocksalt parent Bragg peaks are all highly asymmetric. This asymmetry is characteristic of size-effect distortion due to relaxation of the rocksalt lattice around the defects. In the analysis of Welberry and Christy (1995, 1997), relaxation in the crystal model was carried out using a simple Monte Carlo (MC) algorithm. For simplicity, interstitial atoms were not included in the simulation but were inserted afterwards. An interaction potential was used in which harmonic (Hooke's law) springs connected primary lattice sites in the the $\langle 1\ 0 \rangle$ and $\langle 1\ 1 \rangle$ directions. The MC energy was given by,

$$E = \sum_{q,b} C_{ab}(R_{ab} - d_{ab})^2 \qquad (3)$$

Here, the summation is over all nearest-neighbour pairs of sites in the $\langle 1\ 0 \rangle$ and $\langle 1\ 1 \rangle$ directions. d_{ab} is the instantaneous length of a given inter-site vector. The equilibrium length of the spring, R_{ab}, between a pair of sites ab was assumed to be equal to $(1 + \varepsilon_{ab})\mathbf{a}_0$ for $\langle 1\ 0 \rangle$ springs and $\sqrt{2}(1 + \varepsilon_{ab})a_0$ for $\langle 1\ 1 \rangle$ springs. The strengths of the force constants, C_{ab}, for the $\langle 1\ 0 \rangle$ and $\langle 1\ 1 \rangle$ springs were assumed to be 20 and 100 respectively in arbitrary units. For the $\langle 1\ 0 \rangle$ springs, the distortion parameter ε_{ab} was set to be -0.06 for vectors between a vacant site and an occupied site; +0.02 between two occupied sites; 0.0 between two vacancies. After distortion, this choice of parameters resulted in the mean cation/vacancy vector being reduced by 4%. These values were chosen because they delivered relaxation which matched that observed in the data (Welberry and Christy, 1995, 1997).

For the purposes of the present study, the aim is to establish which aspects of the model obtained from the single crystal analysis could be observed using the PDF methodology. The present paper is necessarily of limited scope and we restrict the study to exploring four key aspects of the model by asking the questions:

Can PDF distinguish between the different cluster types?

Can PDF distinguish between different paracrystalline defect distributions?

Can PDF distinguish between models in which the defect distribution covers the whole or only part of the lattice. Is it sensitive to the size of the regions covered?

Is the PDF sensitive to the size-effect relaxation of the rocksalt lattice around the defects?

Computer simulations

The model simulations were carried out using custom-written Fortran programs (Welberry and Christy, 1997). The programs produced output suitable for *DIFFUSE* (Butler and Welberry, 1992), which was used for calculating the SCDS patterns, and for *DISCUS* (Neder and Wildgruber, 1989; Neder and Proffen, 2008), which was used to calculate PDF traces (and powder diffraction patterns). As a test, in a few cases *DISCUS* was used to calculate the SCDS also, and results agreed with *DIFFUSE*.

The model crystal consisted of a 1024×1024 two dimensional (2D) lattice. This was used to represent 512×512 unit cells of the projected f.c.c. rocksalt lattice. The incommensurate paracrystal array was a 189×189 2D lattice, established by an initial independent simulation. This was superimposed on the model crystal such that defects were centred at sites n, m given by,

$$n = \text{nint}(5.4i + \sigma X_{i,j}),\ m = \text{nint}(5.4j + \sigma Y_{i,j}) \qquad (4)$$

where n, m are indices on the square lattice which corresponds to the $a_0 \times a_0$ repeat of the projected structure. $X_{i,j}$ and $Y_{i,j}$ are arrays of zero mean unit variance Gaussian random variables defining the displacements of individual sites of the paracrystal lattice away from the sites of a perfect lattice. The factor 5.4 provides that the paracrystal has an average lattice spacing of $\sim 2.7\mathbf{a}_0 \times 2.7\mathbf{a}_0$, where $\mathbf{a}_0$ is the average rocksalt lattice spacing and σ scales the displacements relative to this. The indices i, j (in the range 1–189) refer to points on this paracrystal array.

Results

Effect of cluster size

To test for the effect of cluster size, we compared two models which differ only in the type of cluster used, but are otherwise identical. The results are shown in Fig. 5. A paracrystal distribution of defects defined by the parameters $\rho_L = 0.935$, $\rho_T = 0.08$ and $\sigma = 1.7$ was used for the

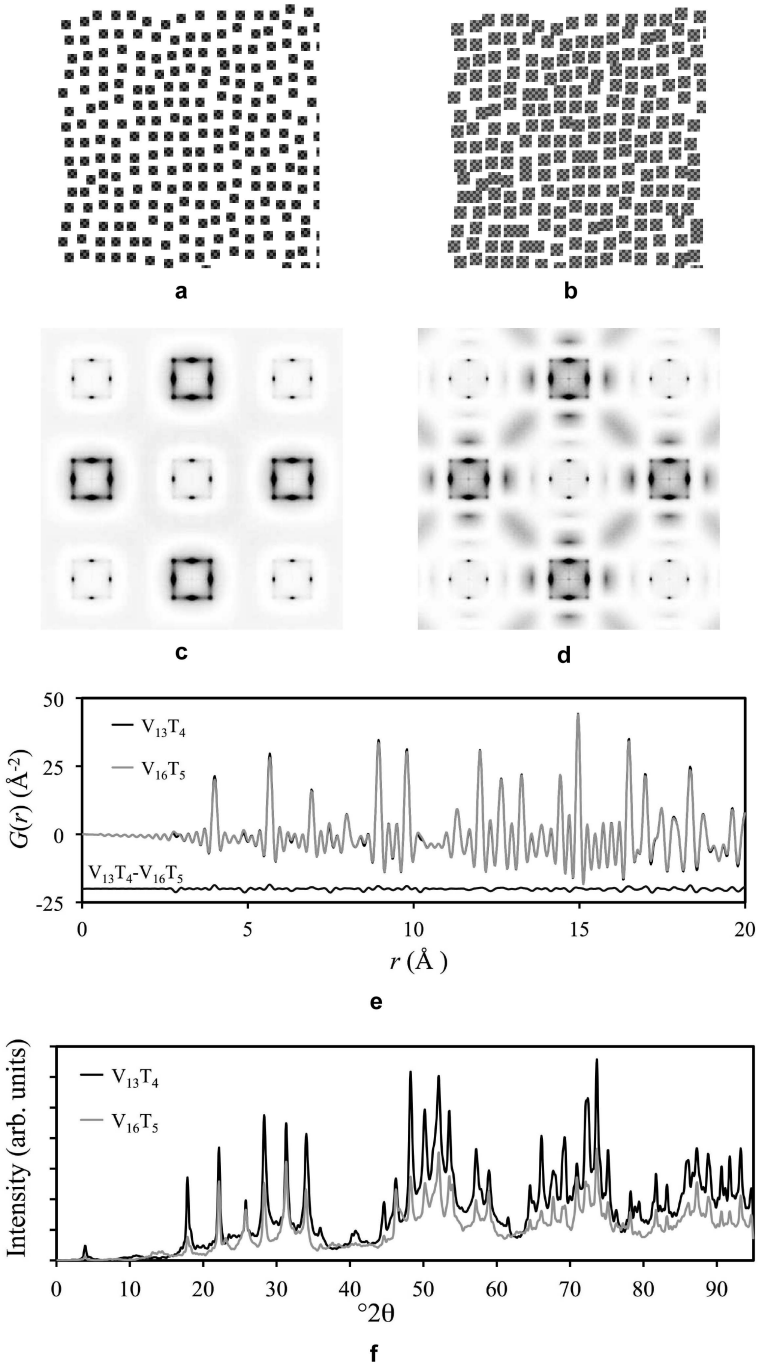

FIG. 5. The effect of cluster size. (*a*,*b*) Real-space distributions of defect clusters for the two models. (*c*,*d*) Corresponding hk0 section SCDS patterns. (*e*) PDF plots for the two models and the difference between them – the traces are very similar, as demonstrated by the high degree of overlap and the small ripples in the difference plot. (*f*) Comparison of the powder diffraction patterns for the two models. See Table 1 for details of the parameters used for the models shown in Figs 5–8.

TABLE 1. Parameters used for the models shown in Figs 5−8. Note that ρ_D was not always specified, but arose indirectly from ρ_L and ρ_T. The value of σ, as used in equation 4, was the same for all examples and corresponds to 31.5% of the mean paracrystal lattice spacing. *C* gives the fraction of the lattice occupied by paracrystal.

Model	ρ_L	ρ_T	ρ_D	Σ	C_{10}	*C*	Size eff. cycles	Defect type
Fig. 5*a*	0.935	0.8	–	1.7	–	1	0	$V_{13}T_4$
Fig. 5*b*	0.935	0.8	–	1.7	–	1	0	$V_{16}T_5$
Fig. 6*a*	0.935	0.8	–	1.7	–	1	0	$V_{13}T_4$
Fig. 6*b*	0.86	0.86	0.86	1.7	–	1	0	$V_{13}T_4$
Fig. 7*a*	0.935	0.8	–	1.7	–	1	0	$V_{13}T_4$
Fig. 7*b*	0.935	0.8	–	1.7	0.2	0.5	0	$V_{13}T_4$
Fig. 8*a*	0.935	0.8	–	1.7	–	1	20	$V_{13}T_4$
Fig. 8*b*	0.935	0.8	–	1.7	0.6	0.5	20	$V_{13}T_4$

two models. For the example shown in Fig. 5*a*, the defect used was $V_{13}T_4$, while for that of Fig. 5*b* the $V_{16}T_5$ defect was used. For each figure, only a small representative portion of each distribution is shown. The fully occupied paracrystalline lattice gave a complete covering of the simulation area.

Figures 5*c* and 5*d* show the corresponding SCDS patterns and distinctive differences are observed. The scattering motif around each rocksalt parent reflection is basically the Fourier transform of the cluster. The $V_{16}T_5$ defect is significantly larger than the $V_{13}T_4$ and its transform consequently goes through its first minimum closer to the centre of the motif, just outside the first order superlattice peak (e.g. at $4\pm\delta\ 0\ 0$). In addition, significant higher-order features can be seen for $V_{16}T_5$, such as peaks at $4\pm2\delta\ 0\ 0$ and other broader regions of diffuse scattering.

In contrast to these SCDS patterns, the PDF plots of the two models shown in Fig. 5*e* are virtually indistinguishable. Some very small differences can be discerned but are not easily interpretable. The corresponding powder patterns do show significant differences (Fig. 5*f*). Differences in peak heights are discernible, but the peaks also appear to reside on differing levels of background scattering. Since all the scattering derives from the model, these differences emphasize that, in a real experiment, it is imperative to fit the 'background' of a properly corrected $S(Q)$ with a function derived from the disorder model, rather than just using a parameteriztion that allows the 'background' to be thrown away.

Different paracrystal distributions

It is primarily the nature of the paracrystalline distribution of defect clusters that gives the motif of scattering around each parent Bragg reflection its characteristic appearance. In this second example, we test whether the PDF and TS method can distinguish such different paracrystalline distributions. The two examples chosen for this test are shown in Figs 6*a* and *b* and their corresponding SCDS patterns are shown in Figs 6*c* and *d*, respectively. These two examples differ only in the values of ρ_L, ρ_T and ρ_D used; σ is the same in each, and the paracrystal array is complete and covers the whole rocksalt lattice. The distribution for Fig. 6*a* has a very strong longitudinal correlation and a weaker transverse correlation, while that in Fig. 6*b* has equally strong transverse, longitudinal and diagonal correlations. Thus, while the diffuse superlattice peaks in Fig. 6*c* are very anisotropic, in Fig. 6*d* they are much more isotropic.

Despite the substantially different paracrystal distribution, the corresponding PDF plots are virtually indistinguishable. Since the clusters themselves are identical, the intra-cluster peaks in $G(r)$ will be the same, but the plots do not reveal any differences deriving from inter-cluster peaks. This is presumably because the average cluster spacings are the same in the two distributions, despite differences in the correlations.

The corresponding powder patterns in Fig. 6*f* do show substantial differences, but it is clear that these differences derive from subtle changes in the shapes and widths of individual peaks.

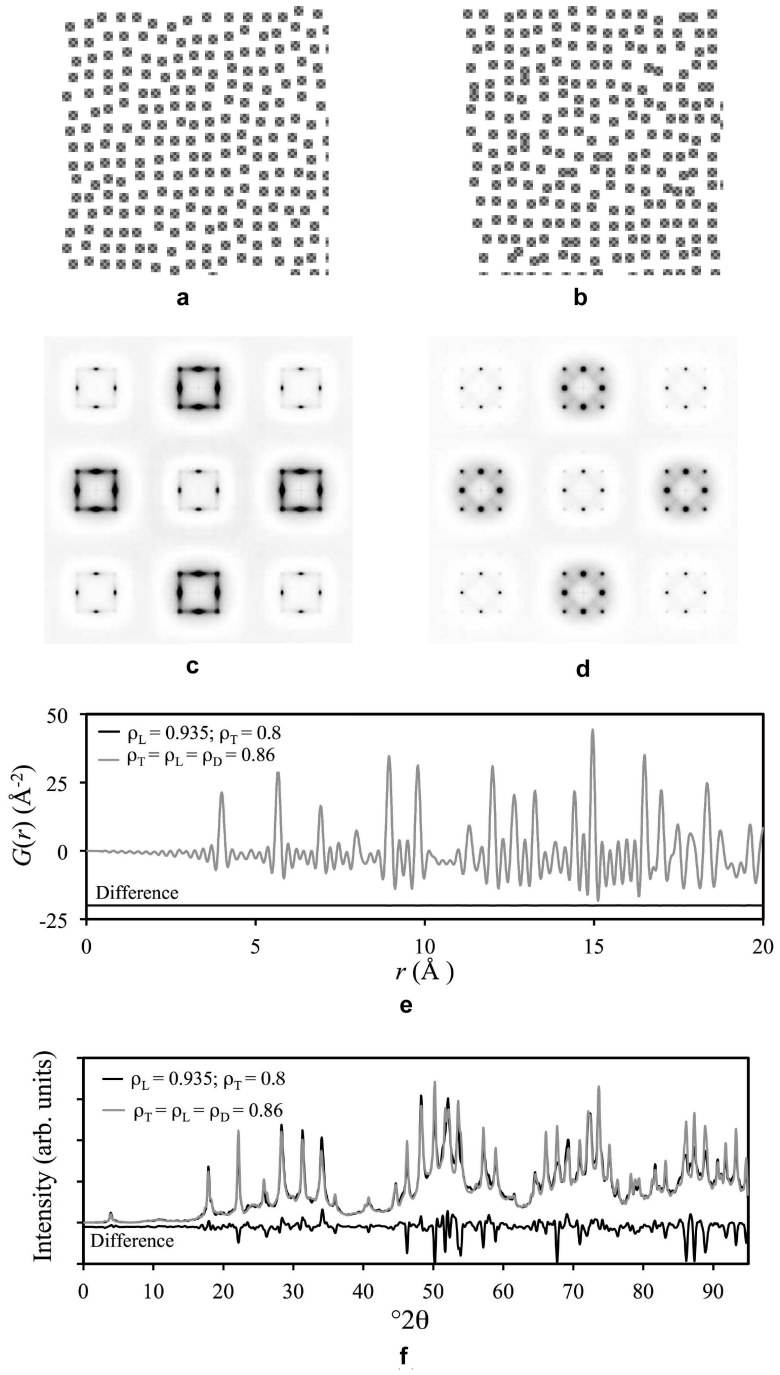

FIG. 6. Different paracrystal distributions. (*a*,*b*) Real-space distributions of defect clusters for the two models. (*c*,*d*) Corresponding *hk*0 section SCDS patterns. (*e*) PDF plots for the two models and the difference between them. (*f*) Comparison of the powder diffraction patterns for the two models. In (*f*), the scale of the difference plot is the same as the diffraction traces, demonstrating that the difference is quite pronounced.

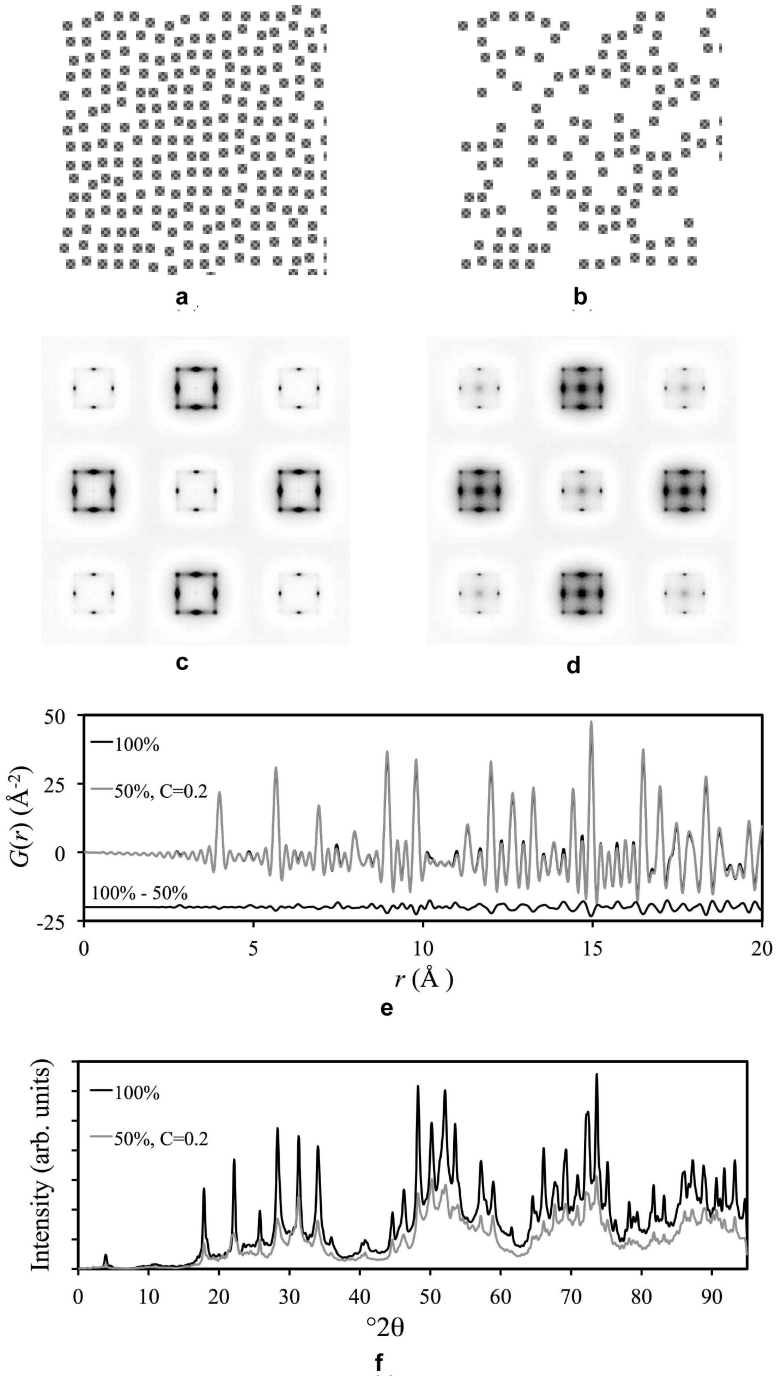

FIG. 7. Domain structure of paracrystal. (*a*,*b*) Real-space distributions of defect clusters for the two models. (*c*,*d*) Corresponding *hk*0 section SCDS patterns. (*e*) PDF plots for the two models and the difference between them. (*f*) Comparison of the powder diffraction patterns for the two models.

Domain structure of paracrystal

The fact that the motif of scattering around the rocksalt parent Bragg peaks in Fig. 4 has a diffuse peak at the centre indicates that the paracrystal lattice does not exist over the whole lattice but occurs only in domains. In this next example, (Fig. 7), we compare the scattering for two simulations in which the same paracrystal distribution is used but in the second defect clusters only occur at 50% of the sites. Moreover, those sites that are occupied tend to occur in domains interspersed with domains where there are no clusters. In the example in Fig. 7*b*, this domain structure has been produced using an Ising model with nearest-neighbour correlation $C_{10} = 0.2$ (see above, the section on the disordered defect structure).

The PDF plots of the two simulations are shown in Fig. 7*e*. It is seen these are very similar at small values of r where intra-cluster vectors dominate, but differ increasingly at larger r, where inter-cluster vectors are increasingly important.

It is remarkable just how different the powder diffraction patterns are, given the similarities of the PDFs. While there is in general a correspondence of peaks, the intensities are much lower in the example where the occupancy is 50% and the correlation forming the domains is weak. The real-space arrangement corresponding to the latter case (Fig. 7*b*) shows that the paracrystalline arrangement is broken up into domains that are only a few unit cells in size, so that the defect distribution is effectively random in a significant proportion of the sample. Figure 7*e* shows the resulting loss of peak intensity, increase in peak width and large background-to-peak ratio, which are as we would expect for a poorly crystalline material.

Experimentally, given that the PDF is derived from the powder pattern, these differences would be apparent to the investigator. However, these results do reflect on the ability of the PDF to constrain a model of the local ordering.

Size-effect relaxation around defects

In this fourth example, we compare two example simulations in which 'size-effect' relaxation is applied around the defect clusters using equation 3. The two examples use the same paracrystal distribution with $\rho_L = 0.935$, $\rho_T = 0.08$ and $\sigma = 1.7$, but for the first (Fig. 8*a*), the paracrystal is complete while for the second (Fig. 8*b*) the paracrystal has a domain structure with 50% occupancy and a value of $C_{10} = 0.6$. (The effect of C_{10} can be illustrated by comparing Fig. 8*b* with 7*b*.) In both cases, the relaxation produces a characteristic transfer of intensity from the high-angle side of the motif to the low (cf. Fig. 7*c*). Note that in Fig. 8*d*, the intensity in the diffuse central peak is also displaced toward the low-diffraction angle side.

The PDF plots for these two examples are shown in Fig. 8*e*. The redistribution of interatomic vector lengths can be seen clearly in the shapes of individual PDF peaks. The effect is most pronounced for the first example, which contains the complete paracrystal of defects. For the second example, which contains only domains of paracrystal with large areas of defect free rocksalt lattice, the redistribution of vector lengths is less noticeable. With the size-effect algorithm applied for only a relatively small number of MC cycles, the average interatomic distances in this rocksalt part (~50%) of the crystal will be largely unaffected by the relaxation. The effect on the average vector length distribution of only part of the crystal being occupied by paracrystal is to dilute the effects from the paracrystal regions, which results in the shapes of the PDF peaks being much closer to those observed for the pure rocksalt structure.

The corresponding powder patterns are shown in Fig. 8*f*. As for the previous example (Fig. 7), the patterns have a relatively large background-to-peak ratio, particularly that having the disordered domain structure. There are now substantial differences in peak heights.

Conclusions

In the Results section above, we showed how different aspects of a model of the complex disordered structure of wüstite affect the PDF and powder diffraction pattern. It is clear even from this rather limited set of examples that some aspects of the model have a strong effect on the PDF, the powder diffraction pattern or both, while others do not. This general observation is confirmed by numerous other examples that have been examined but which are not reported here for the sake of brevity. While each aspect of the disordered model gives a clear, interpretable effect in the SCDS pattern, the corresponding manifestations in the PDF and powder diffraction are less amenable to such simple interpretation.

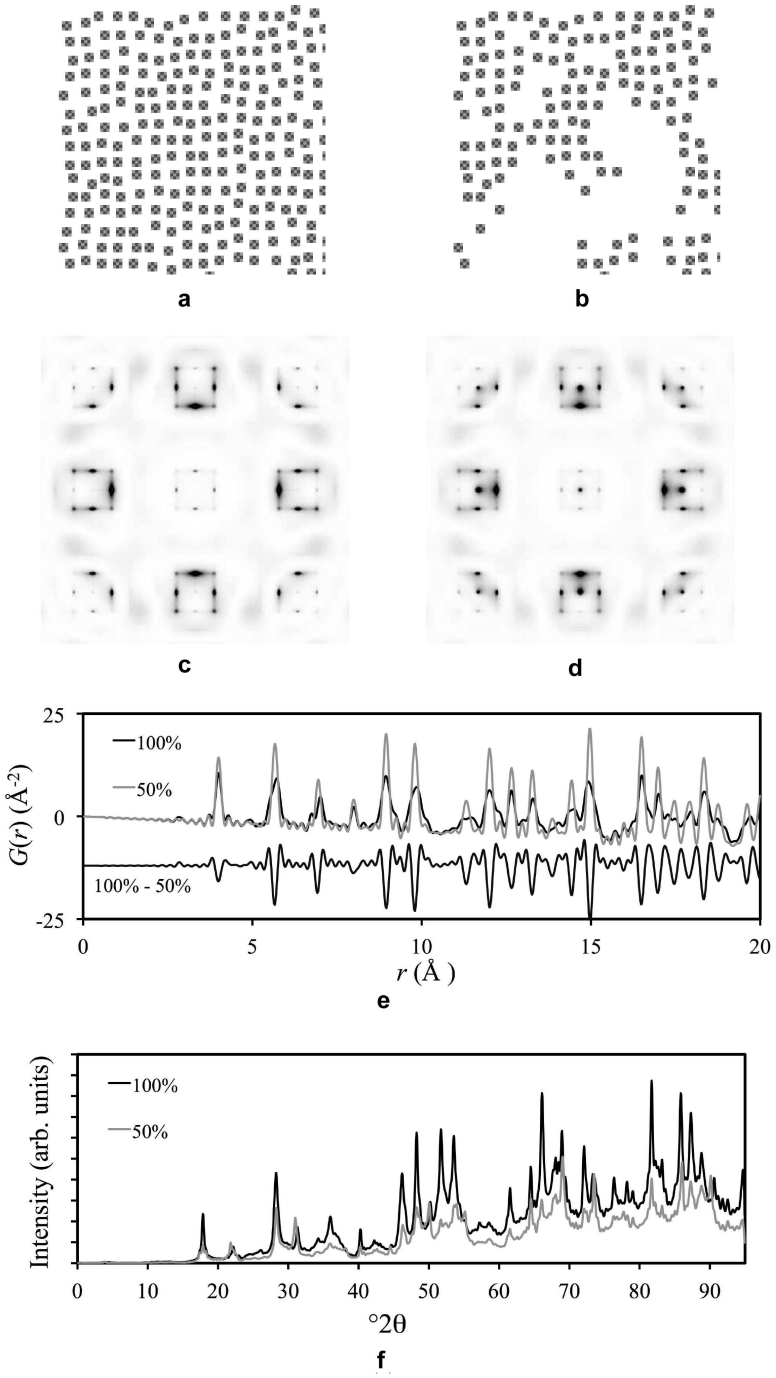

FIG. 8. Size-effect relaxation around defects. (*a*,*b*) Real-space distributions of defect clusters for the two models. (*c*,*d*) Corresponding *hk*0 section SCDS patterns. (*e*) PDF plots for the two models and the difference between them. (*f*) Comparison of the powder diffraction patterns for the two models.

Nevertheless, it is clear that PDF and powder diffraction do contain significant information regarding the disordered structure.

The results presented here suggest that PDF data are sensitive to those aspects of the models that have a significant effect on the populations of interatomic spacings, such as changing the fraction of the sample occupied by defect clusters or changing the degree or type of 'size effect' relaxation. These are very significant qualities of the material, which are largely or wholly inaccessible using conventional diffraction methods that rely on the Bragg peaks alone.

The PDF is less able to allow investigation of the correlation structures in the samples if these do not have a substantial interaction with interatomic separations. For example, changes in the type of the defect clusters or in the way the clusters order (e.g. whether they tend to aggregate or disperse randomly) have little effect on the PDF unless the size-effect relaxation couples these changes to a change in the distribution of interatomic spacings.

On the other hand, differences in SCDS patterns can be pronounced even when PDFs are almost the same – a good example is seen in Fig. 6, where the paracrystalline parameters are varied, resulting in major qualitative changes to the SCDS but almost negligible change to the PDF. This result occurs, even when size-effect is applied to these two models, because the fraction of the model undergoing 'size-effect' relaxation is virtually unchanged between the two cases. Although the relationship of one defect cluster to the next changes, the population of defect clusters does not change and neither does the fraction of the sample undergoing relaxation. As a result there is minimal change in the population of interatomic spacings and the PDFs are very similar.

The scope of the present study has been limited to an exploration of the effect on the PDF of various attributes of a model for the disordered structure of wüstite that was established by fitting to the SCDS observations. A further development would be to use the PDF data to develop a structural model directly. The present work makes it clear that if this is attempted, then it is important that both the PDF and the powder diffraction pattern should be fitted simultaneously (Tucker *et al*., 2007). Also, the background of the powder pattern might usefully be fitted using a function derived from the SRO model. That the intensities of Bragg reflections and background in the powder diffraction patterns depend on the model parameters suggests that it may be desirable to place the data and the model on absolute and directly comparable scales. The present work indicates that while PDF most certainly delivers insights that conventional (Bragg scattering) studies cannot, SCDS also provides insights that PDF cannot. Qualitatively exploring the PDFs, powder diffraction patterns and reciprocal space sections of real-space models of local ordering provides insight into the analysis of PDF and powder diffraction data, even when SCDS data is not available.

Acknowledgements

We gratefully acknowledge support of the Australian Research Council in the form of a Discovery Project Grant. Computational time at NCF, Canberra is also gratefully acknowledged. Use of the Advanced Photon Source was supported by the U.S. Department of Energy, Office of Science, Office of Basic Energy Sciences, under Contract No. DE-AC02-06CH11357.

References

Billinge, S.J.L. and Levin, I. (2007) The problem with determining atomic structure at the nanoscale. *Science*, **316**, 561–565.

Butler, B.D. and Welberry, T.R. (1992) Calculation of Diffuse Scattering from Simulated Crystals: a Comparison with Optical Transforms. *Journal of Applied Crystallography*, **25**, 391–399.

Garstein, E. and Cohen, J.B. (1980) Comments on the defect structure in wustite. *Journal of Solid State Chemistry*, **33**, 271–272.

Hazen, R.M. and Jeanloz, R. (1984) Wüstite ($Fe_{1-x}O$): A review of its defect structure and physical properties. *Reviews of Geophysics*, **22**, 37–46.

Huq, A., Welberry, T.R. and Bozin, E. (2010) Advances in structural studies of materials using scattering probes. *MRS Bulletin*, **35**, 520–530.

Juhas, P., Cherba, D.M., Duxbury, P.M., Punch, W.F. and Billinge, S.J.L. (2006) Ab initio determination of solid-state nanostructure. *Nature*, **440**, 655–658.

Koch, F. and Cohen, J.B. (1969) The defect structure of $Fe_{1-x}O$. *Acta Crystallographica B*, **25**, 275–287.

Michel, F.M., Ehm, L., Antao, S.M., Lee, P.L., Chupas, P.J., Liu, G., Strongin, D.R., Schoonen, M.A.A., Phillips, B.L. and Parise, J.B. (2007) The structure of ferrihydrite, a nanocrystalline material. *Science*, **316** 1726–1729.

Neder, R.B. and Proffen, Th. (2008) *Diffuse Scattering and Defect Structure Simulations: A Cook Book*

using the Program DISCUS. Oxford University Press, Oxford, UK.

Neder, R.B. and Wildgruber, U. (1989) DISCUS, ein Interaktives Programm zur Simulation von Defektstrukturen und Diffuser Streuung. *Zeitschrift für Kristallographie*, **186**, 209.

Proffen, Th. (2006) Analysis of disordered materials using total scattering and the atomic pair distribution function. *Neutron Scattering in Earth Sciences*, **63**, 255−274.

Proffen, Th. and Billinge, S.J.L. (1999) PDFfit, a program for full profile structural refinement of the atomic pair distribution function. *Journal of Applied Crystallography*, **32**, 572−575.

Rietveld, H.M. (1969) A profile refinement method for nuclear and magnetic structures. *Journal of Applied Crystallography*, **2**, 65.

Roth, W.L. (1960) Defects in the crystal and magnetic structures of ferrous oxide. *Acta Crystallographica*, **13**, 140−149.

Schweika, W., Hoser, A., Martin, M. and Carlson, A.E (1995). The defect structure of ferrous oxide $Fe_{1-x}O$. *Physical Review B*, **51**, 15771−15788.

Tucker, M.G., Keen, D.A., Dove, M.T., Goodwin, A.L. and Hui, Q. (2007) RMCprofile: Reverse Monte Carlo for polycrystalline materials. *Journal of Physics: Condensed Matter*, **19**, 335218.

Welberry, T.R. and Christy, A.G. (1995) A paracrystalline description of defect distributions in wüstite, $Fe_{1-x}O$. *Journal of Solid State Chemistry*, **117**, 398−406.

Welberry, T.R. and Christy, A.G. (1997) Defect distribution and the diffuse X-ray diffraction pattern of wüstite, $Fe_{1-x}O$. *Physics and Chemistry of Minerals*, **24**, 24−38.

Welberry, T.R. and Christy, A.G. (1998) About short- and long-range orderings in wüstites, $Fe_{1-x}O$. *Physics and Chemistry of Minerals*, **26**, 81−82.

Welberry, T.R., Miller, G.H. and Carroll, C.E. (1980) Paracrystals and growth-disorder models. *Acta Crystallographica Section A*, **36** 921−929.